POLITECNICO DI TORINO
Repository ISTITUZIONALE

Design of the cryogenic loop for the superconducting toroidal-field magnets of the Divertor Tokamak Test

Original
Design of the cryogenic loop for the superconducting toroidal-field magnets of the Divertor Tokamak Test / Lisanti, F., Angelucci, M., Bonifetto, R., Michel, F., Duri, D., Frattolillo, A., Froio, A., Iaboni, A., Migliori, S., Roussel, P., Zanino, R.. - In: CRYOGENICS. - ISSN 0011-2275. - ELETTRONICO. - 136:(2023), p. 103757. [10.1016/j.cryogenics.2023.103757]

Availability:
This version is available at: 11583/2985238 since: 2024-01-18T18:12:24Z

Publisher:
ELSEVIER SCI LTD

Published
DOI:10.1016/j.cryogenics.2023.103757

Terms of use:

This article is made available under terms and conditions as specified in the corresponding bibliographic description in the repository

Publisher copyright

(Article begins on next page)

18 November 2026

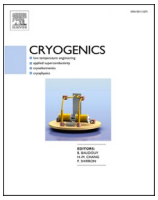
Cryogenics 136 (2023) 103757



Contents lists available at ScienceDirect

Cryogenics

journal homepage: www.elsevier.com/locate/cryogenics





Design of the cryogenic loop for the superconducting toroidal-field magnets of the Divertor Tokamak Test

Fabrizio Lisanti [a], Morena Angelucci [b], Roberto Bonifetto [a,*], Frédéric Michel [c], Davide Duri [c], Antonio Frattolillo [b,d], Antonio Froio [a], Andrea Iaboni [e], Silvio Migliori [b], Pascal Roussel [c], Roberto Zanino [a]

[a] NEMO group, Energy Department, Politecnico di Torino, C.so Duca degli Abruzzi 24, 10129 Torino, Italy
[b] ENEA, Via E. Fermi 45 I, 00044 Frascati, Roma, Italy
[c] Univ. Grenoble Alpes, CEA, IRIG, Département des Systèmes Basses Températures, 17 Rue des Martyrs, F-38054 Grenoble, Cedex, France
[d] DTT S.C. a r.l, Via E. Fermi 45 I, 00044 Frascati, Roma, Italy
[e] Eni SpA, piazzale Enrico Mattei 1, 00144 Roma, Italy

ARTICLE INFO

Keywords:
DTT
TF cryogenic circuit design
Thermal–hydraulic modelling
4C code
Optimization
Mitigation

ABSTRACT

The design of the cryogenic circuit for the toroidal field magnets has a relevant role in the overall costs of the DTT cryogenic plant (or cryoplant), hence numerical tools can be useful to investigate and to compare different configurations for the TF cooling circuit in support of the selection of the most suitable one. The system-level cryogenic circuit module of the validated thermal–hydraulic 4C code is adopted in this work to model the DTT TF cooling system. At first, the model of the reference circuit layout is implemented and simulated during the plasma pulsed operation of the DTT machine, highlighting the necessity to reduce the heat load transferred to the refrigerator due to the large power consumption of the cold compressor. In view of the above, different TF circuit layouts and optimization strategies are presented, including mitigation strategies for the smoothing of the peak heat load to the refrigerator, leading to a reduction of the cold compressor power up to the 66% with respect to that computed for the reference TF cryogenic circuit layout.

1. Introduction

The Divertor Tokamak Test (DTT) facility [1,2,3,4] is being built at ENEA Frascati (Italy), to address the development of a power exhaust system capable to handle the large heat fluxes expected to be deposited in fusion reactors on the plasma facing components.

DTT will be a compact and flexible fusion experiment relying on low-temperature superconducting magnets for the plasma confinement. The magnets will be cooled to their operating temperature by supercritical helium (SHe) at 4.5 K and ~ 0.5 MPa, distributed by cryogenic circuits composed by supply and return cryolines, heat exchangers (HX), control valves and a cold circulator (CC). These circuits need to be designed to handle both the pulsed heat loads deposited in the coils by AC losses and nuclear particles during the operation of the tokamak and the static heat transferred by conduction and radiation from the cryostat to the magnets. To smooth the heat load suffered by the refrigerator, which should operate as much as possible at a constant thermal load, the heat will be transferred to a thermal buffer, i.e. a saturated liquid He bath (as done for JT60-SA [5]).

In this work, thermal–hydraulic numerical models are used to support the design of the DTT cryodistribution system for the toroidal field (TF) magnet system. In particular, the cryogenic circuit module of the 4C code [6] is reliably adopted, in view of its successful validation history [7] including also predictive exercises [8,9]. The model of several different circuit layouts is implemented in the 4C code and simulated during the plasma pulsed operation, comparing the evolution and peak values of the heat load transferred from the cryogenic circuits to the thermal buffer.

The paper is organized as follows: as a first step, the criteria and algorithm used for the sizing of the pipes of the cryolines are reported, based on the pressure drop and static heat load. Then different cryodistribution layouts are introduced, as well as their model and simulation setup; finally, the results of the different options are compared in a dedicated section, using also the entire 4C code to confirm the capability

* Corresponding author at: Dipartimento Energia, Politecnico di Torino, Corso Duca degli Abruzzi 24, 10129 Torino, Italy. Tel.: +39 011 0904443.
E-mail address: roberto.bonifetto@polito.it (R. Bonifetto).

https://doi.org/10.1016/j.cryogenics.2023.103757
Received 7 July 2023; Received in revised form 12 September 2023; Accepted 17 October 2023
Available online 18 October 2023
0011-2275/© 2023 The Author(s). Published by Elsevier Ltd. This is an open access article under the CC BY license (http://creativecommons.org/licenses/by/4.0/).

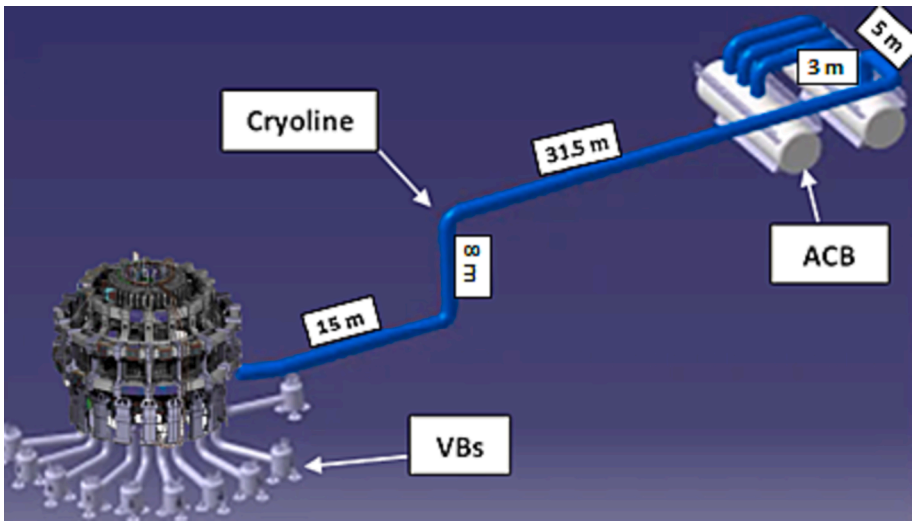


Fig. 1. CAD view of the DTT cryoline.

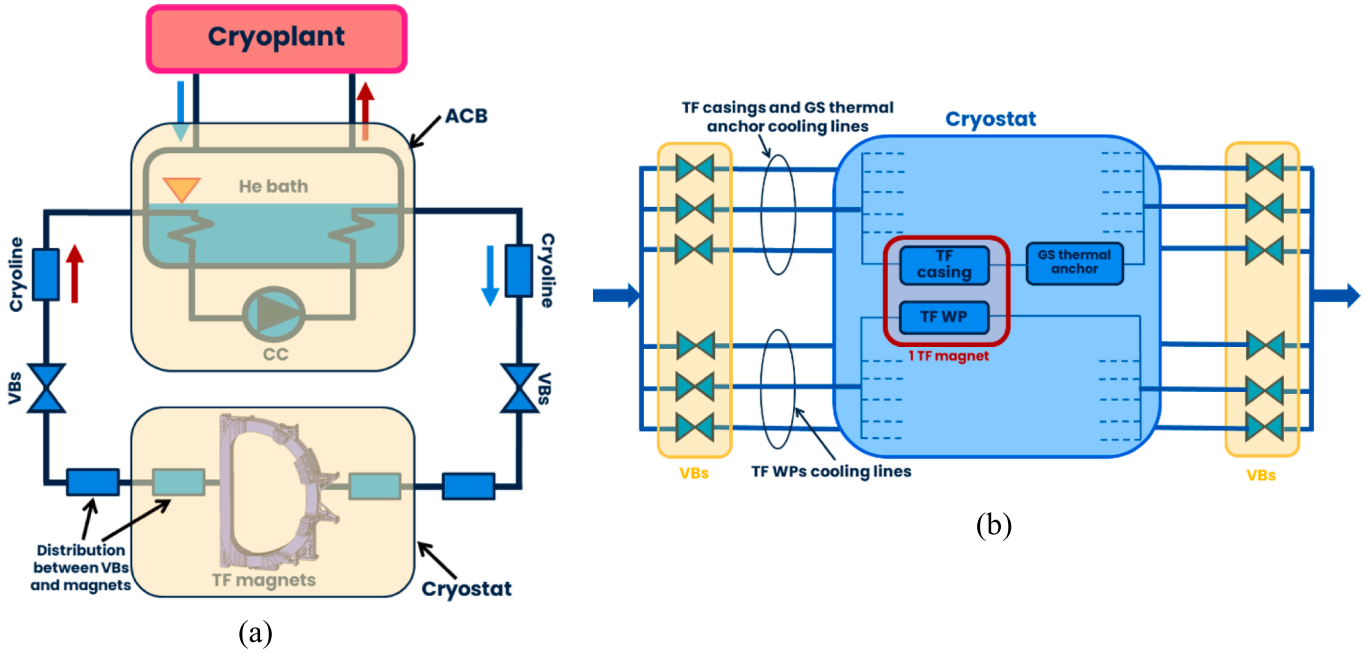


Fig. 2. Simplified scheme of the TF cryogenic circuit: (a) view of the whole circuit and (b) detail of the cryodistribution between VBs and magnets.

of the different layouts to guarantee the minimum temperature margin in the TF coils.

2. Preliminary sizing of the main cryodistribution lines

To dimension the main cryodistribution lines of the TF cooling circuit, a preliminary 1D thermal–hydraulic analysis is performed. Pressure drop and radiative heat load are computed for each line, parametrically changing the pipe diameter among values taken from standard dimensions of stainless steel pipes. The resulting pipe diameters and heat loads are given as inputs to the system-level model of the entire TF cryogenic loop.

The main component for the distribution of SHe to the cryogenic clients of the DTT tokamak is the cryoline (shown in Fig. 1), which runs for ~ 60 m from the Auxiliary Cold Box (ACB) inside the refrigerator building – where the LHe bath and CCs are placed – to the Valve Boxes (VBs) located around the cryostat of the tokamak. The DTT cryoline contains all the supply and return lines of the different cryogenic circuits, including those for the TF conductors and structures. To reduce the radiative heat load coming from the external environment, the loop pipes inside the cryoline are surrounded by a thermal shield (inner diameter of 0.8 m), which is cooled by the supply line of the 80 K loop by heat conduction.

From the VBs, three lines for the conductors and three for the casings (each feeding six TF magnets) supply SHe to in-cryostat collectors, where the coolant is then distributed to each of the 18 TF winding packs and 18 TF casings, for a total of 36 lines. The same holds for the return lines from the magnets to the VBs. For this work, an average length of 30 m is assumed for the lines connecting VBs and in-cryostat collectors, and an average length of 2 m for the lines feeding each TF magnet from the collectors. Fig. 2a shows a simplified scheme of the entire TF circuit with the main cryogenic lines, with a detail of the distribution between VBs and magnets (Fig. 2b).

The Colebrook equation has been used to compute the friction factor f:

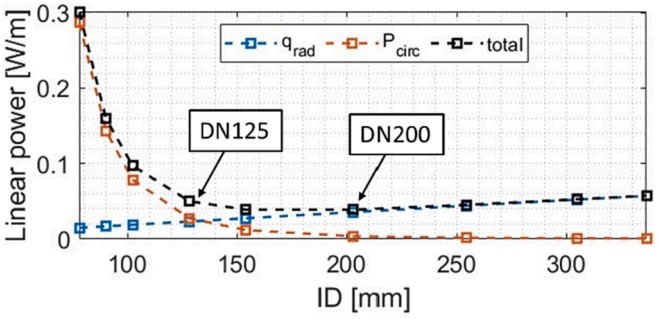


Fig. 3. Sizing example for the TF supply line inside the cryoline: Heat load (blue line), power consumption due to pressure drop (orange line) and sum of the two (dashed-black line) per unit pipe length as function of the pipe diameter; squares correspond to standard stainless steel pipe diameters. (For interpretation of the references to colour in this figure legend, the reader is referred to the web version of this article.)

$$\frac{1}{\sqrt{f}} = 2.0\log\left(\frac{\omega}{3.7} + \frac{2.51}{Re\sqrt{f}}\right)$$

where ω is the relative roughness of pipes inner surface, assumed equal to 0.0003, and Re is the Reynolds dimensionless number. Moreover, localized pressure losses have been considered for the supply and return pipes inside the cryoline due to four 90° elbows (see Fig. 1), for which a loss coefficient K_{loc} equal to 0.7 is conservatively assumed [10]. The overall pressure loss Δp_{loss} along pipes is then computed as:

$$\Delta p_{loss} = \left(f\frac{L}{D} + K_{loc}\right)\frac{\rho v^2}{2}$$

where L and D are the pipe length and inner diameter, respectively, ρ is the helium density and v the flow velocity.

Radiative heat loads are computed under the simplifying assumption that each pipe interfaces only with the external surfaces at 80 K (cryoline, VBs and in-cryostat thermal shields), neglecting the presence of other pipes or other items. For the TF supply and return lines in the cryoline, for instance, this is a conservative assumption, since they will interface with the distribution lines of the other cryogenic loops, which are at temperature $\leq$ 80 K. Moreover, the presence of reflective Multilayer Insulation (MLI) foils wrapped around the pipes outer surface is considered in this work to reduce the heat load on the SHe distribution lines. From datasheet of commercially available MLI (Beyond Gravity Space [11] Coolcat 2) for cryogenic applications, reporting a heat flux of 0.05 W/m^2 for 10 foils and a temperature range of 77 K to 4 K, a value of MLI emissivity equal to 0.043 has been deduced. At present, the conductive heat losses of the supports (spacers every 1 m) and vacuum interfaces are neglected.

The net radiative heat exchange (in W) between loop pipes and 80 K surfaces is computed as

$$q_{rad} = \frac{\sigma\left(T^4 - T_{sur}^4\right)}{R}$$

where σ is the Stefan-Boltzmann constant, T_{sur} is the thermal shield temperature, T is the temperature of the pipe outer surface, assumed equal to the fluid temperature inside the pipe, and R is the resistance to radiation exchange between the two surfaces. The latter is a function of the surfaces of heat transfer S_{wet} (hence, it depends on the pipe diameter), of the emissivity of the pipe and thermal shield surfaces (ε_{pipe} and ε_{TS}, respectively, conservatively assumed equal to 0.4), of the MLI foils emissivity ε_{MLI}, and of the view factors F_1 between pipe and MLI and F_2 between MLI and thermal shield (both equal to 1 due to the assumption of neglecting the presence of other pipes). The resistance R is computed as:

$$R = \frac{1-\varepsilon_{pipe}}{\varepsilon_{pipe}S_{wet,pipe}} + \frac{1}{S_{wet,pipe}F_1} + \frac{1-\varepsilon_{TS}}{\varepsilon_{pipe}S_{wet,TS}} + 2\frac{1-\varepsilon_{MLI}}{\varepsilon_{MLI}S_{wet,MLI}} + \frac{1}{S_{wet,MLI}F_2}$$

For the selection of the suitable diameter for the TF cryogenic loop pipes, a trade-off between pressure drop (and, consequently, CC power consumption) – decreasing as the diameter increases – and radiative heat load – increasing as the diameter increases – is needed. As an example, Fig. 3 shows the results of the analysis for the in-cryoline distribution line of the reference layout of the TF cooling circuit (presented in section 3.1), where heat load and CC power consumption are compared as a function of the diameter. In this case, the diameter corresponding to the minimum of the total power, defined as the sum of the two curves (dashed-black line), is a DN200, which is the optimum for the trade-off between pressure drop and heat load. However, this diameter value lies on a region where the total power is quite flat, such that the small gain in terms of a lower pressure drop compared to smaller diameters does not justify the larger stainless steel mass required (which results in larger energy consumption during the cooldown transient). In view of this, the idea is to select a smaller diameter, with respect to the one corresponding to the minimum, that still falls inside the flat region of the total power curve of Fig. 3. Therefore, a DN125 pipe has been chosen for the in-cryoline distribution line; despite a ~ 28 % increase in the total power with respect to the minimum point, the absolute linear power remains small (~0.05 W/m, therefore with a negligible impact on the refrigerator balance) and the chosen pipe diameter still guarantees a low pressure drop of ~ 2 mbar along the 60 m of the cryoline.

In Table 1 are listed the diameters (and related heat loads) of the supply cryodistribution lines for the reference TF cooling circuit, selected with the criteria described above. The same pipe diameters have been selected for the return lines, for which a minor (negligible) difference on the computed heat loads with respect to the supply lines is observed, due to the different pressure and temperature of the SHe.

3. System-level analysis of the reference TF cooling circuit

3.1. Reference cryodistribution layout

A simplified scheme of the reference layout for the TF magnets cooling is shown in Fig. 4, consisting of a single hydraulic circuit – fed by a CC – providing SHe to the conductors and casings of the 18 TF magnets. The SHe from the cryoline is split inside the VBs in two parallel

Table 1
Inputs and results of the sizing analysis for the main cryogenic supply lines of the reference TF cooling circuit layout.

Cryodistribution line type		Number of pipes	Pipe length [m]	Mass flow rate per pipe [g/s]	Inlet conditions assumed: temperature [K]/ pressure [bar]	**Selected pipe diameter**	**Radiative heat load per pipe [W/m]**
In-cryoline loop pipe		1	60	864	4.5 / 5	**DN125**	**0.023**
TF WPs cooling branch	Between VB and in-cryostat collector	3	30	228	4.5 / 5	**DN50**	**0.010**
	Between collector and magnet	18	2	38	4.5 / 5	**DN20**	**0.004**
TF casings cooling branch	Between VB and in-cryostat collector	3	30	60	4.5 / 3.2	**DN25**	**0.005**
	Between collector and magnet	18	2	10	4.5 / 3.2	**DN15**	**0.004**

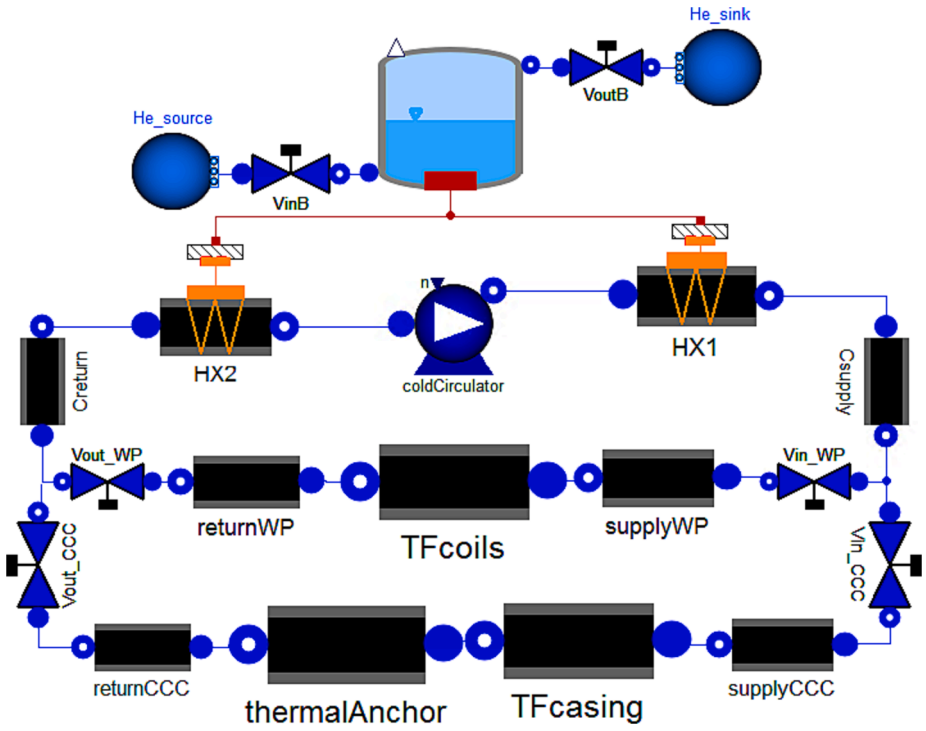


Fig. 4. Scheme of the reference TF cooling circuit model.

branches, one feeding the Winding Pack (WP) cooling channels and the other the Casing Cooling Channels (CCCs) and gravity support (GS) thermal anchor. Since the pressure drop along the hydraulic channels of the conductors is much larger than that along the CCCs, a large pressure drop across the lamination valve upstream the CCCs (*Vin_CCC*) is needed to equilibrate the SHe flow between the two parallel branches. Note that inducing the additional pressure drop downstream the CCCs would be disadvantageous – if compared to the pressure drop in the valve upstream the CCCs – since a larger helium pressure in the casing channels would result in a lower He specific heat. Two HXs, placed in the ACB upstream and downstream the CC, transfer the heat removed from the TF magnets to a saturated LHe bath, which aims to smooth the pulsed heat loads from the TF cooling circuit, since the He refrigerator should operate as much as possible at a constant load.

When only steady state heat loads are suffered by the magnets, a total SHe mass flow rate of ~ 860 g/s flows in the circuit, which is split in 680 g/s for the TF conductors and 180 g/s for the TF casings and GS thermal anchor. This corresponds to a mass flow rate of ~ 3.8 g/s per hydraulic channel in the WP and ~ 2.5 g/s per channel in the CCCs. The friction factor in the WP channels is deduced in the model by assuming a nominal operating point (2 bar pressure drop at the nominal He mass flow rate of ~ 3.8 g/s per channel), while for the CCCs the Colebrook equation is used. The nominal operating point for the conductors was confirmed by tests performed on DTT TF conductor samples. Moreover, the helium bath is assumed to work at a pressure of ~ 1.2 bar, corresponding to a saturation temperature of 4.45 K, which results in a SHe temperature of 4.54 K at the inlet of the TF cooling channels. This is the minimum He bath overpressure allowing to push the helium back to the warm compressor (whose suction is at ambient pressure), overcoming the pressure losses in the regenerative HX series, without the need of an additional cold compressor.

The geometrical inputs adopted for the TF WPs, CCCs and GS thermal anchor are listed in Table 2. Note that, since the CCCs are carved in the stainless steel structure of the TF casing, the value of the outer diameter is assumed such that the resulting cross-section of the channel walls is equal to the actual TF casing cross-section.

The presence of other cryogenic circuits, as that for the cooling of poloidal-field coils and central solenoid, is not accounted for in this work since they are only slightly coupled with the TF circuit through the He bath. For this reason, the only effect of the optimization of the TF circuit, discussed in section 4, is to change the heat load delivered to the thermal buffer, and therefore slightly modify its operating temperature during transients.

Table 2
Geometrical data used for WP, CCC and GS thermal anchor models.

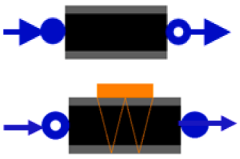
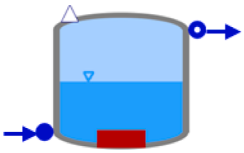
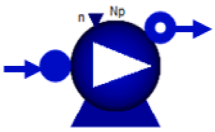
Component	Number of parallel cooling channels (for 1 TF magnet) [-]	Channel length [m]	Channel inner diameter [mm]	Channel outer diameter [mm]
TF WP [12]	10	108	12.3	30.4
TF casing [12]	4	12	8	146.7
GS thermal anchor	1	10.8	10	14

3.2. Model and simulation setup

The system-level model for the TF cooling circuit of the DTT tokamak has been developed using the cryogenic circuit module of the 4C code, a state-of-the-art numerical tool developed at Politecnico di Torino for the thermal–hydraulic modelling of relevant transients for superconductive magnet system of fusion machines. The 4C circuit module was developed using the CryoModelica library, based on the Modelica modelling language [13], which allows to easily develop dynamic models of complex systems due to its object-oriented and dynamic nature, and relies on the open-source ThermoPower [14] and ExternalMedia [15] libraries for the development of components models and for an efficient interface with external codes computing He properties, respectively.

The components adopted in this work for the development of the TF cryogenic circuit of DTT – such as pipes, LHe bath, valves, CCs and HXs – are presented in Table 3. For all the components, dynamic balance equations are solved, allowing the simulation of relevant transients of

Table 3
Main components (available in the 4C code) adopted for the TF cryogenic circuit model.

Component	Symbol	Assumptions	Main equations solved
Pipe / HX		1D finite-volume discretization	1D mass, momentum and energy conservation
Valve		0D, volume neglected, isenthalpic transformation	Mass and energy conservation
LHe bath		0D, thermodynamic equilibrium between phases, only saturated vapor is extracted	Mass and energy conservation for both phases
CC		0D, isentropic efficiency η_{iso} constant (assumed equal to 100% here), volume neglected	Mass and energy conservation, characteristic

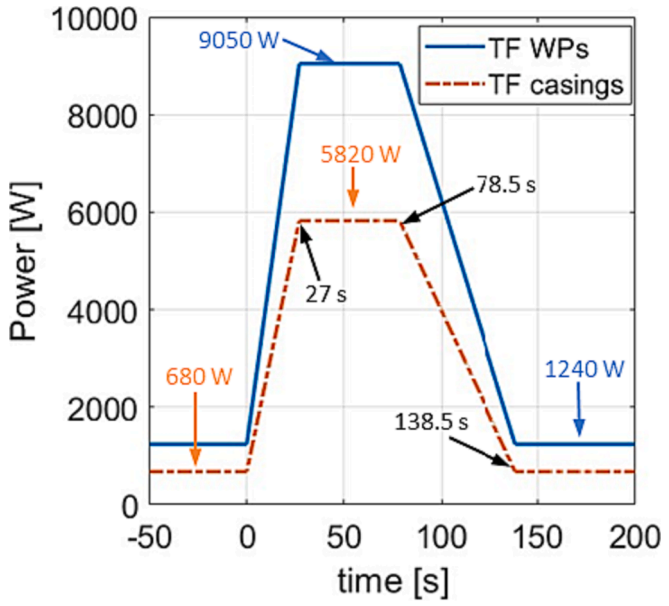


Fig. 5. Heat load pulse shape for TF WPs and casings. From 140 s to 3600 s no dynamic heat load is applied.

the TF cryogenic circuit operation; more details about the model implementation can be found in [6].

The model is simulated during the plasma operation of the DTT tokamak (with a period of 3600 s), when pulsed heat loads are deposited in the TF WPs and casing. The nuclear heat load adopted for the simulations is the same used in [12], evaluated in [16] based on the 2020 version of the SN (Single-Null) scenario, but foreseeing no neutron shield and an increased heat load at the outboard region to account for the removal of the port collars. Static heat loads have been re-evaluated with respect to those reported in [12] using a 1D model for conduction in the GS and improving the estimation of the thermal shield emissivity. Fig. 5 shows the shape of the heat loads deposited in the conductors and casing of all 18 TF coils during one plasma pulse of a duration of ~ 100 s.

Table 4
Main inputs for the simulation of the reference TF circuit model.

Total mass flow rate [kg/s]	Mass flow rate in TF WPs cooling branch [kg/s]	Mass flow rate in TF casings and GS thermal anchor cooling branch [kg/s]	Nominal Δp along conductors [bar]	Conductors inlet pressure [bar]	LHe bath temperature [K]
864	684	180	2	5	4.45

The only dynamic heat load that is missing in the model, to the best of authors knowledge, is the one due to eddy currents in the casing. Moreover, a static heat load of 25 W is assumed for the thermal anchor of each of the 18 GSs, which are not included in Fig. 5 because they are given as input directly to the thermal anchor model. The static heat load on the TF WP is a static conductive heat load from the casings through the ground insulation.

Regarding the CC model, a realistic, parabolic characteristic is assumed:

$$H = -1.5435 \cdot 10^{7} Q^{2} - 1.8987 \cdot 10^{5} Q + 1.5888 \cdot 10^{3}$$

where H is the specific energy in [J/kg] and Q is the volumetric flow rate in [m^3/s].

The models for HXs, warm compressors, turbines and other components of the He refrigerator are not included in this work. As shown in Fig. 4, the saturated LHe is fed by an ideal pressure source – supplying He at 16 bar and 4.5 K – and the He vapor is extracted by a pressure sink at 1.1 bar placed downstream the thermal buffer (which is operated at 1.2 bar). The He flow rate to the thermal buffer is controlled by a proportional-integral controller, having proportional coefficient equal to 2 and integration time equal to 20 s, which regulates the opening of a control valve (VinB in Fig. 4, upstream the thermal buffer) to maintain a steady level of helium of 70% inside the LHe bath during the simulated transient. Table 4 summarizes the main inputs used for the simulations.

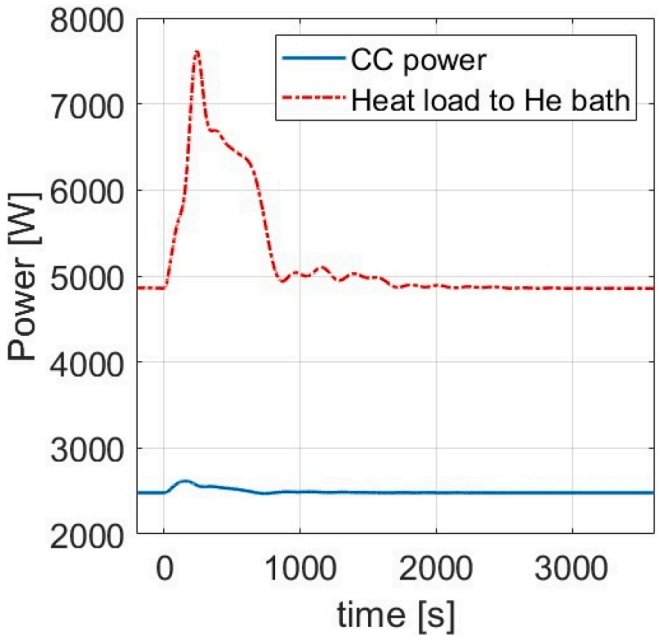


Fig. 6. Reference layout results: Thermal power delivered to the He bath (red curve) and CC power consumption (blue curve). (For interpretation of the references to colour in this figure legend, the reader is referred to the web version of this article.)

3.3. Results

The results of the simulation of a plasma pulse for the reference TF cooling loop layout are shown in Fig. 6, in terms of thermal load transferred to the He bath at the HXs and CC power. A very large peak heat load to the thermal buffer of 7.6 kW is obtained during the plasma pulse, decreasing to 4.9 kW during the dwell, i.e. when the pulse is extinguished and only the static loads are present. Approximately 50% of the steady state heat load to the bath during the dwell is due to the cold circulator work (slightly less than 2.5 kW). Removing the ~ 2.5 kW from CC power, the remaining steady state heat load delivered to the He bath is composed by the power deposited in the conductors and casing (~1.95 kW) and that from the GS thermal anchor (~0.5 kW), other than a small contribution due to radiative heat loads in the cryolines.

The first proposal to reduce such a large contribution to the steady state heat load to the refrigerator, without changing the circuit layout, is to reduce the CC pressure head (and consequently the SHe mass flow rate in the WP). This can be achieved by a lower (but constant) CC rotational speed, assuming a constant efficiency. However, the reduction of the mass flow rate in the WP cooling channels has a negative impact on the temperature margin for the conductors, limiting the allowable reduction of the CC pressure head, see Fig. 7. The lowest possible pressure head for which the temperature margin is computed to be still acceptable is around 1.5 bar.

4. Alternative TF cooling circuit layouts

The results obtained for the reference layout highlight the necessity to investigate different optimization strategies for the cooling of the TF magnet system, to reduce the heat load to the refrigerator, in particular the CC power (accounting for ~ 50% of the steady state heat loads to the He bath), and therefore the operational cost. The following optimization strategies are explored:

1. Use of two separate loops for the TF WPs and for the casings (see Fig. 8). The advantage of having a separate loop for the components with reduced pressure drops (i.e. casings and GS thermal anchor) is that, with respect to the reference layout, the large pressure drop across the lamination valve upstream the CCCs is avoided, resulting in a reduced CC power for that loop. Since the cryogenic circuits for WPs and casings are separate, two additional cryodistribution lines inside the main cryoline are needed.
2. Reduction of the CC pressure head with subcooling of the thermal buffer to compensate the negative effect on the conductors temperature margin shown in section 3.3 above. A reduction of the He bath operating temperature to 4.2 K has been assumed, resulting in a reduction of the SHe temperature at the inlet of the WPs to ~ 4.3 K. This solution, however, has a cost: the reduction of the He bath

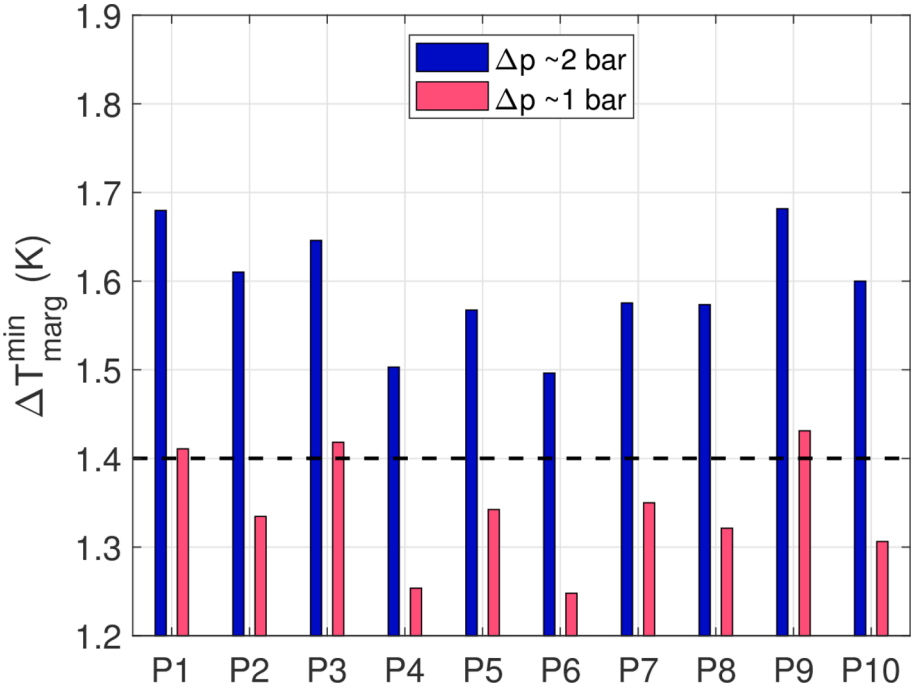


Fig. 7. Temperature margin for the 10 pancakes at different operating conditions.

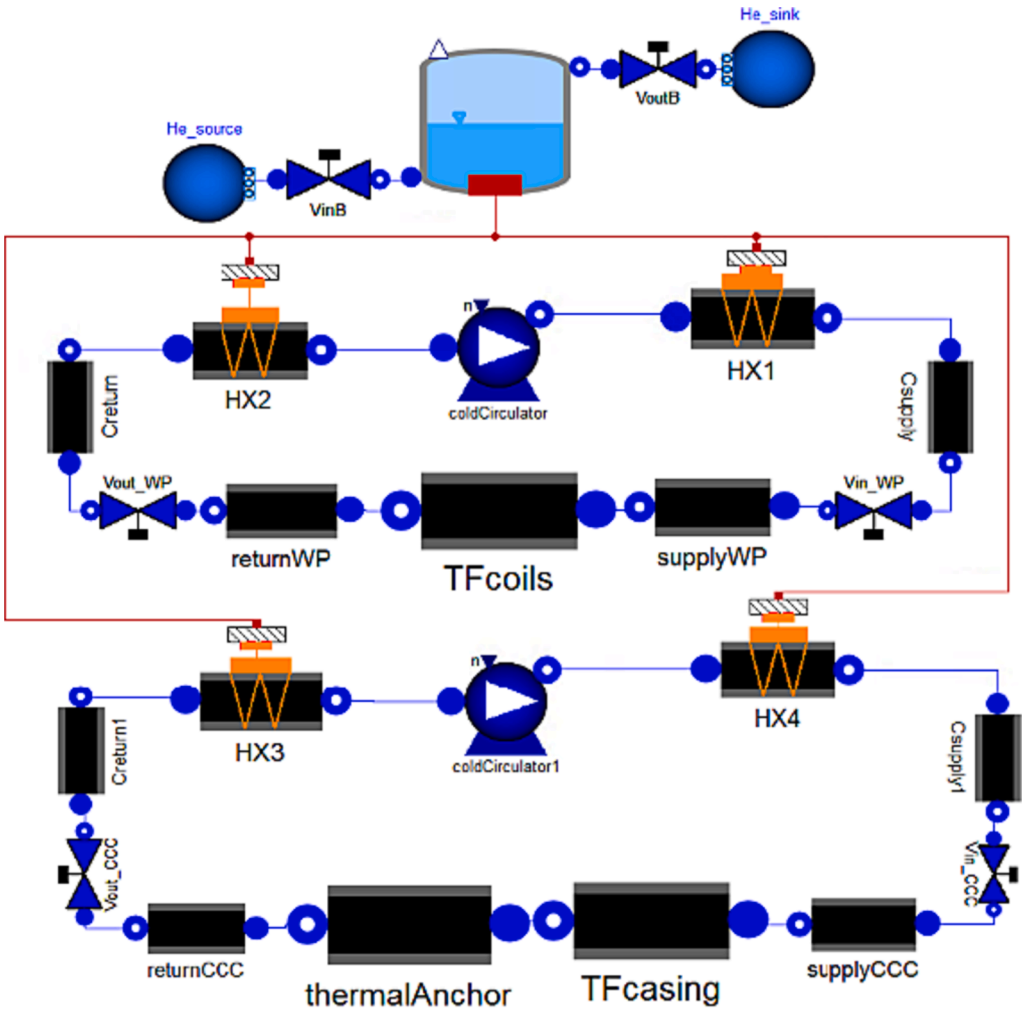


Fig. 8. Scheme of the model for the optimization strategy 1: separate circuits for TF conductors and casings.

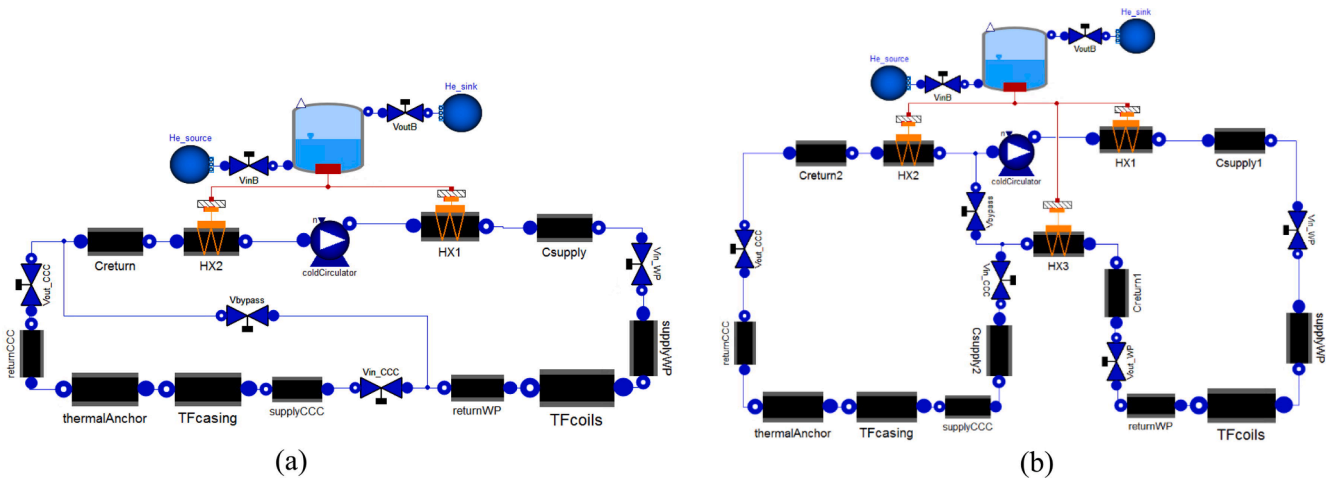


Fig. 9. Scheme of the models for the optimization strategy 3: (a) connection of the CCCs in series to the WPs without (a) and with (b) intermediate cooling of SHe upstream the CCCs.

operating temperature at 4.2 K entails a bath pressure of 0.99 bar, which means that a cold compressor is needed downstream the He bath to push the He back to the warm compressor through the regenerative HX series. In perspective, it could be interesting to consider the possibility to have an additional, smaller subcooled He bath thermally coupled with the HX downstream the CC, while still maintaining the coupling of the other HX to the main bath at 4.5 K.

3. Connection of the CCCs in series to the WP (see Fig. 9a). As for the optimization strategy 1, also in this case the large pressure drop across the lamination valve upstream the CCCs is avoided, with the

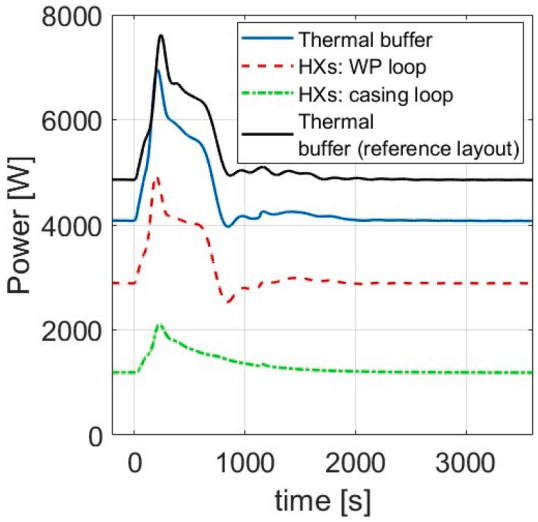


Fig. 10. Results of the optimization strategy 1: thermal power delivered to the He bath, compared to that computed for the reference layout (black line), and power exchanged at the HXs of the two separate loops.

advantage of having a single cooling circuit for the TF (hence, no additional CC and cryolines are required) with a reduced total SHe mass flow rate, corresponding to that flowing in the TF conductors branch. Since the flow rate needed for the cooling of TF structures and GS thermal anchor is lower than the that required by the WP, a fraction of the SHe mass flow rate exiting the TF conductors cooling channels bypasses the casing cooling line. Similarly to the optimization strategy 1, a reduction of the CC pressure head with subcooling of the thermal buffer to 4.2 K is adopted; in particular, the mass flow rate in the conductors (hence, the total flow rate in the circuit) is reduced to ~ 600 g/s, resulting in a Δp along the WP of 1.5 bar. The connection of the CCCs in series to the conductors cooling channels results in a larger SHe temperature inside the casings, hence a variation in the circuit layout involving the addition of an intermediate heat exchanger, placed upstream the CCCs, is also investigated (as shown in Fig. 9b); in this case, however, two additional cryolines are required as for the optimization strategy 1.

For the alternative TF circuit layouts, the diameters (and related static heat loads) of the main cryodistribution lines are selected following the criteria described in Section 2 for the sizing of the pipes.

4.1. Results and comparison

4.1.1. Optimization strategy 1

The simulations performed for the optimization strategy 1 resulted in a total power consumption of the two CCs of ~ 1.7 kW when only steady state loads are present, almost 0.8 kW lower than the reference layout. Furthermore, the impact of the CC of the casing cooling circuit (~60 W) is negligible if compared to the WP CC power, since it has very low pressure head and a He mass flow rate ~ 4 times smaller than that of the WP circuit.

Fig. 10 shows the evolution of the total heat load to the He bath, compared to that computed for the reference layout, together with the loads transferred at the HXs of the two loops. The resulting peak load to the He bath, slightly lower than 7 kW, is reduced by ~ 600 W (in view of the lower CC steady state heat load) if compared to that computed for the reference layout; however, it can be noticed that the peak loads transferred by the two circuits are almost simultaneous. Therefore, an optimization strategy to smooth the overall peak power to the refrigerator is possible by delaying the peak power transferred by one of the two circuits.

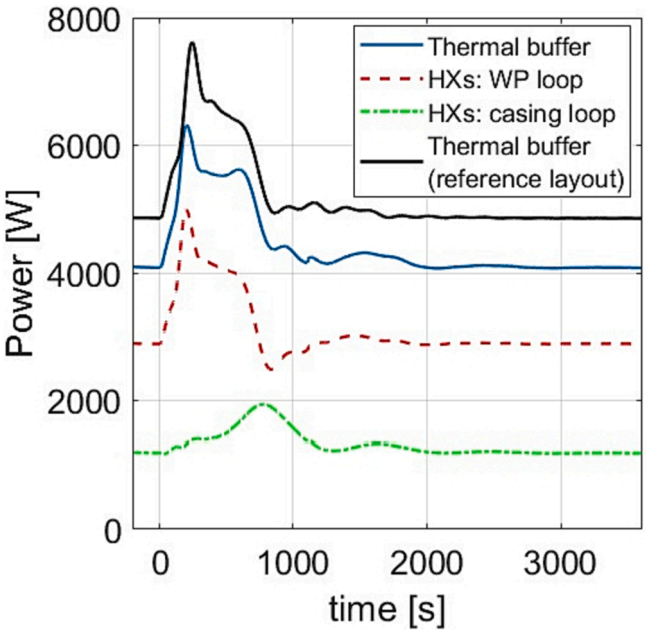


Fig. 11. Option 1A results: thermal power transferred to the He bath, compared to that computed for the reference layout (black line), and power exchanged at the HXs of the two separate loops.

In view of the above, two options have been considered to delay the peak heat load coming from the TF casing cooling circuit:

Increase the return in-cryoline pipe dimensions,
Reduce the CC rotational speed during the heat load pulse.

4.1.1.1. Option 1A: Increased in-cryoline pipe dimensions. The idea behind this strategy is to increase the transit time of the SHe flow through the return line inside the cryoline to delay the heat transfer to the He bath. To do so, both diameter and length of the pipe have been increased: to effectively delay the peak load from the casings circuit (to an instant when the pulse from the TF WPs circuit is almost extinguished) a pipe with a DN90 diameter and additional 90 m length is required.

The results of the simulation are shown in Fig. 11: the pulsed heat load from the casings circuit is shifted forward, resulting in a smoother evolution of the power transferred to the refrigerator with a peak value of 6.3 kW, hence reducing it almost by 0.7 kW with respect to the non-optimized configuration. However, the main drawback of this optimization option is the more complex layout for the cryodistribution due to the larger dimensions of the return cryoline for the casing cooling loop, which, in addition, will undergo a larger radiative heat load of 2.5 W over the 150 m pipe length (~4 times larger than that of the nominal pipe).

4.1.1.2. Option 1B: Reduced CC rotational speed. A second optimization strategy to delay the peak load transferred from the casing circuit is to reduce the CC rotational speed for a sufficient time span during the plasma pulse, reducing the mass flow rate and hence increasing the transit time in the return cryoline.

The most effective results, shown in Fig. 12, have been obtained for a CC rotational speed reduction to ¼ of its nominal value for 800 s starting from the beginning of the plasma pulse. The computed peak heat load to the thermal buffer in this case is equal to 5.9 kW, resulting in a further reduction of 0.4 kW compared to the option 1A.

With this optimization strategy, the TF casings are used as a thermal buffer where heat is deposited during the pulse and transferred over a

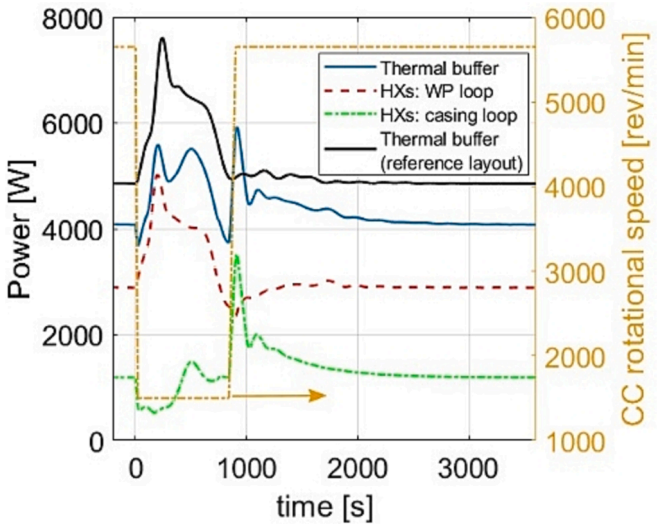


Fig. 12. Option 1B results: (left axis) thermal power transferred to the He bath, compared to that computed for the reference configuration, and power exchanged at the HXs of the two separate loops, and (right axis, yellow line) rotational speed evolution of the casing circuit CC. (For interpretation of the references to colour in this figure legend, the reader is referred to the web version of this article.)

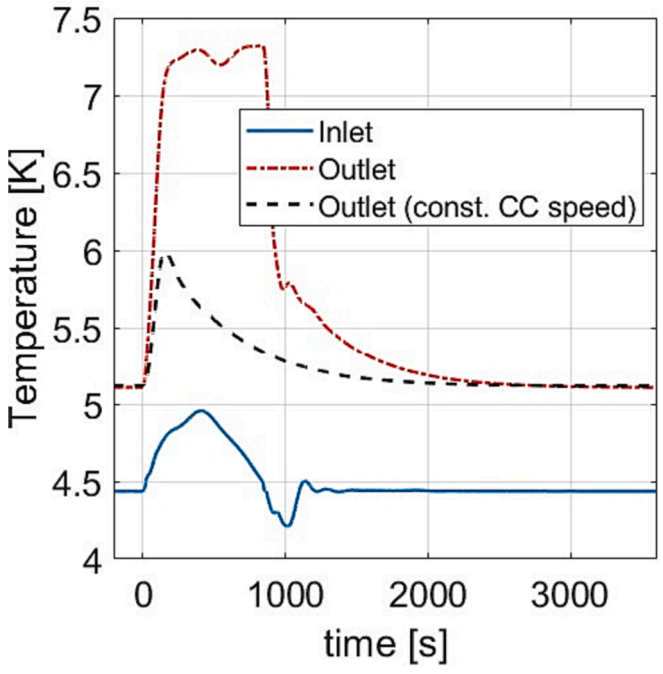


Fig. 13. Option 1B: He temperature evolution at the inlet and outlet of the CCCs.

longer period to the He bath. This is clearly noticeable in Fig. 13, which shows the temperature evolution at the casing cooling channels inlet and outlet: the outlet temperature (dash-dotted red line) reaches a peak value of ~ 1.3 K larger than that of the case with constant CC rotational speed (dashed black line), maintained for a longer time span (~800 s). The inlet temperature drops below 4.5 K (around 1000 s) as an effect of the depressurization of the SHe loop, which is in turn induced by the heat transfer to the He bath in the HX downstream the coil.

Similar optimization strategies for the smoothing of the power transferred to the He bath, by delaying the arrival of the heat loads from the TF coils, are analysed also in [17,18,19], including the variation of

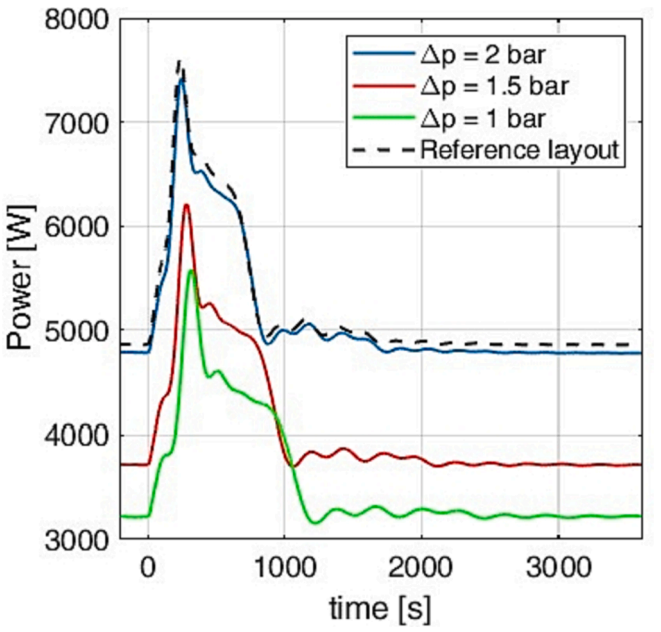


Fig. 14. Results comparison for 3 different CC pressure head values in the case of a He bath operated at 4.2 K: thermal power transferred to the thermal buffer. Also the power to the He bath computed for the reference layout is shown (black dashed line) for a comparison.

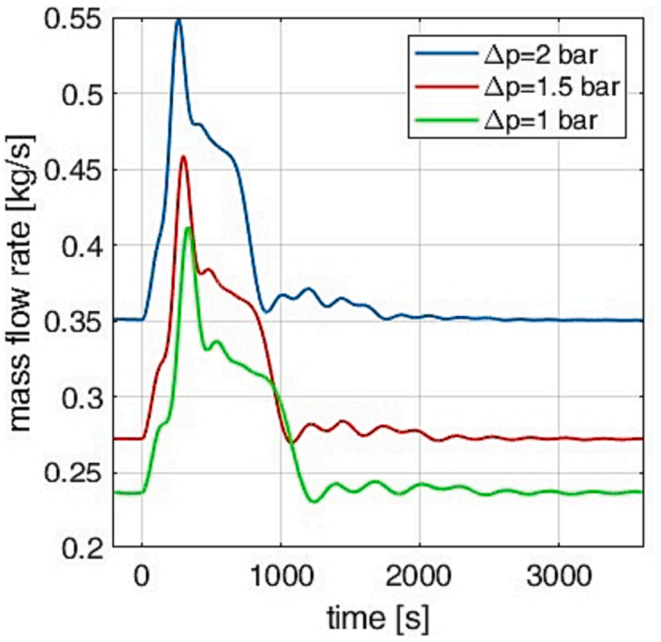


Fig. 15. Vapor mass flow rates at the He bath outlet for 3 different CC pressure head values.

the circulator speed or the use of controlled bypass valves.

4.1.2. *Optimization strategy 2*

The model of the TF cooling loop with a 4.2 K He bath (optimization strategy 2) is run for three values of the CC rotational speed, resulting in a pressure drop along the WPs channels of 2 bar (nominal Δp value), 1.5 bar and 1 bar, respectively. Results obtained by the simulations highlighted a 66 % reduction in the power consumption of the CC with respect to the reference layout, in the case of a Δp of 1 bar along the WP (from 2.48 to 0.84 kW). As a result, a significant reduction of the heat

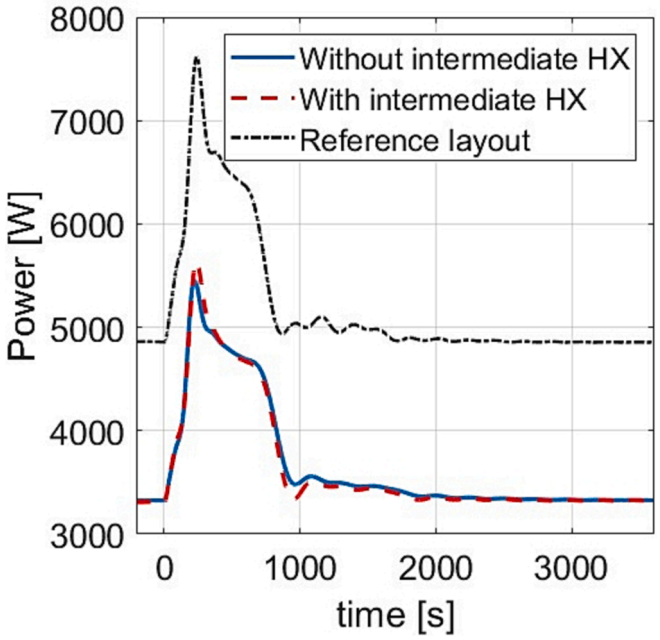


Fig. 16. Results for the optimization strategy 3 in terms of evolution of the power transferred to the thermal buffer; results for both cases with and without intermediate cooling are compared to that obtained for the reference layout.

load transferred to the refrigerator is observed, as shown in Fig. 14, with a peak value 2 kW lower and a baseload 1.6 kW lower than that obtained for the reference configuration.

As a result of the reduction of the CC rotational speed, the total He mass flow rate in the circuit undergoes a reduction of ~ 240 g/s from the case with $\Delta p = 2$ bar to that with $\Delta p = 1$ bar across the WP cooling channels. Moreover, the He vapor mass flow rate exiting the bath has been computed for the three cases, as shown in Fig. 15, and will be useful for the sizing of an adequate cold compressor.

4.1.3. Optimization strategy 3

Finally, the models for the optimization strategy 3 have been run for both cases with and without intermediate cooling upstream the CCCs: as expected, a significant reduction of the circulating power, for both cases around 950 W, is observed with respect to the 2.5 kW computed for the reference layout (~62% reduction). Note that a small difference of ~ 3 W is obtained between the two cases, due to the pressure drop along the additional cryodistribution lines needed for the intermediate cooling of the SHe upstream the CCCs. Because of the pump work reduction, the steady state heat load (equal to ~ 3.3 kW) is reduced by ~ 1.6 kW compared to the reference layout. As shown in Fig. 16, the peak heat load to the He bath during the plasma pulse is almost 5.5 kW if no intermediate cooling is considered, otherwise the peak increases to 5.6 kW.

In spite of the large reduction in the CC power (~62%) and thermal power delivered to the He bath with respect to the reference layout, this TF circuit layout brings some limitations during the cooldown transient. In fact, to keep the maximum thermal gradient in the TF coils structures below an acceptable threshold during the whole transient, the cooldown rate is required to slow down with respect to the reference circuit configuration.

4.1.4. Summary of the results

The heat load to the He bath and CC power obtained for the different circuit layouts and mitigation strategies are summarized in Table 5. In addition to peak and steady state values for the heat load transferred to the thermal buffer, also the average power and energy deposited during one plasma cycle, and the resulting power of the refrigerator at room temperature (assuming the ideal case of a Carnot cycle), are reported. The maximum reduction, with respect to the reference case, of the energy deposited in the He bath (and of the refrigerator power at room temperature) are obtained in the case of the optimization 2 (subcooled bath and reduced dm/dt) with a Δp along the conductors of 1 bar.

4.2. Temperature margin analysis

The value of the minimum temperature margin in each pancake is reported in Fig. 17a for the nominal case and compared to that with a reduced LHe bath temperature. In particular, the subcooling would in principle allow to halve (down to ~ 1 bar) the pressure head required to the cold circulator, even though a pressure head of at least ~ 1.2 bar would be required to have the same temperature margin distribution as in the nominal case. The optimization strategy 3 (series connection of the WP and CCCs without inter-cooling) requires a slightly higher pressure head (up to ~ 1.5 bar), but still smaller than the nominal one, while the total mass flow can be reduced in view of the series connection.

Fig. 17b reports the evolution of the He temperature at the inlet of the HX upstream the cold circulator. Note that all the optimized strategies show a lower temperature peak, which combined with a smaller mass flow rate results in a lower power transferred to the LHe buffer. In particular, the series connection of the WP and CCCs has the advantage of shifting the temperature peak arriving from the WP (as it has to pass also through the casing), thus naturally (partially) smoothing the peak temperature.

5. Conclusions and perspective

The models available in the system-level cryogenic circuit module of the 4C code have been adopted in this work to model the TF cooling loop for the DTT tokamak, and dynamic simulations during the plasma pulsed operation of the machine were performed to assess the heat load

Table 5
Summary of the results obtained for the different TF circuit layouts and optimization strategies.

	CC steady state power [kW]	Steady state heat load to He bath [kW]	Peak heat load to He bath [kW]	Average heat load to He bath [kW]	Energy deposited in He bath (1 plasma cycle) [MJ]	Power at 300 K (Carnot cycle) [kW]
Reference layout	2.48	4.86	7.62	5.21	18.8	342
Optimization 1	1.70	4.08	6.96	4.42	15.9	290
Optimization 1 (increased pipe dimensions - option 1A)	1.70	4.08	6.32	4.43	16	291
Optimization 1 (reduced CC speed - option 1B)	1.70	4.08	5.92	4.42	15.9	290
Optimization 2 ($\Delta p_{WP} = 2$ bar)	2.40	4.78	7.42	5.13	18.5	361
Optimization 2 ($\Delta p_{WP} = 1.5$ bar)	1.34	3.72	6.22	4.07	14.6	287
Optimization 2 ($\Delta p_{WP} = 1$ bar)	0.84	3.22	5.58	3.57	12.8	251
Optimization 3 (no intercooling)	0.95	3.33	5.46	3.67	13.2	258
Optimization 3 (with intercooling)	0.96	3.32	5.63	3.66	13.2	258

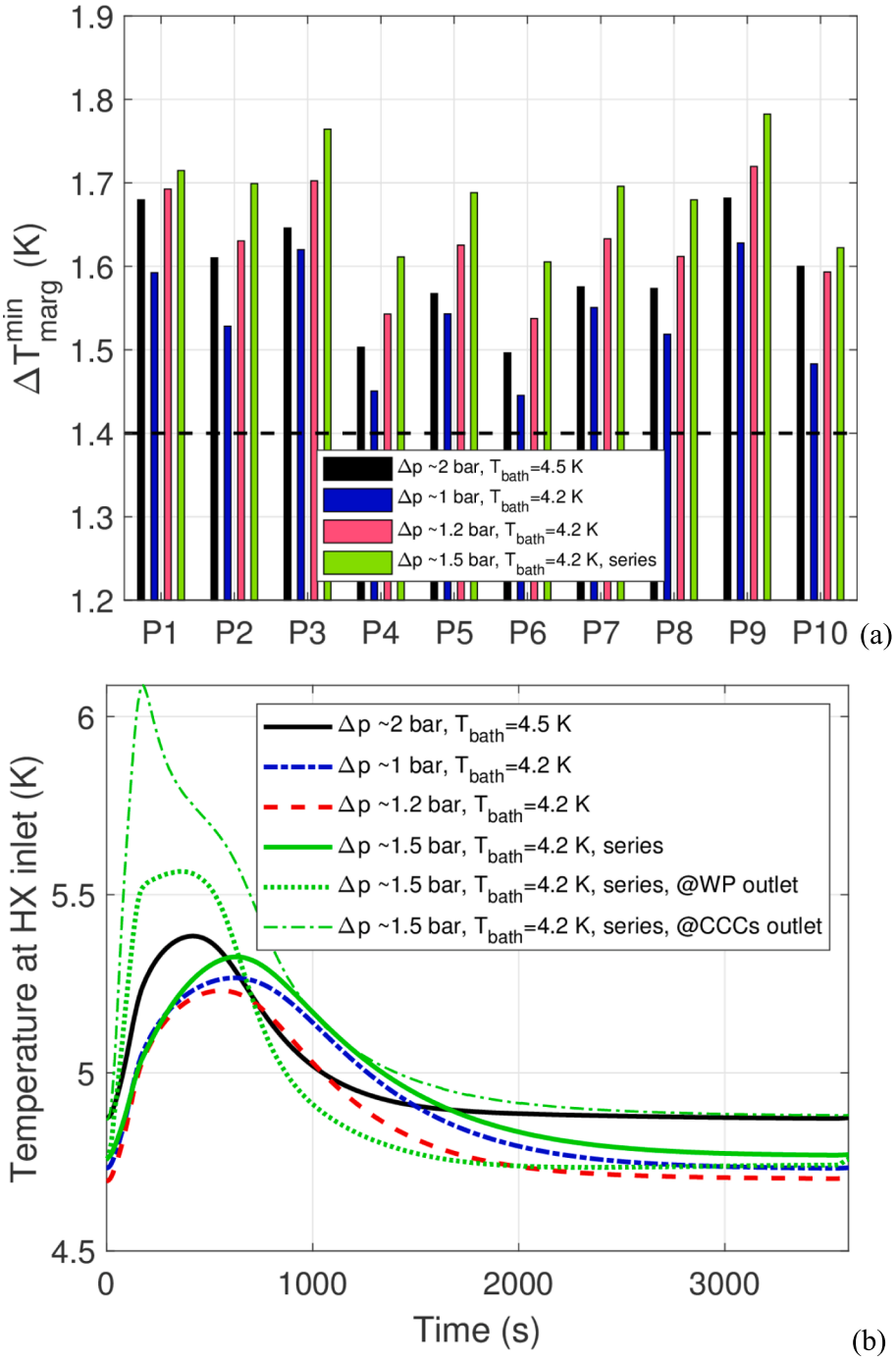


Fig. 17. (a) Temperature margin for the 10 pancakes and (b) evolution of the temperature at the HX inlet for different options. In (b) the Temperature at the WP and CCCs outlet is also reported for the optimization strategy 3 (without inter-cooling).

transferred to the thermal buffer and investigate different optimization strategies.

At first, the initial proposal for the TF circuit layout, consisting of a single circuit for the cooling of TF WPs and TF casings in parallel, has been investigated. Results showed a peak heat load of 7.6 kW during the plasma pulse, decreasing to 4.9 kW when only steady state heat loads are present. To reduce the CC power consumption, which, for the reference TF cryogenic circuit layout, accounted for ~ 50% of the steady state heat load to the thermal buffer, different optimization strategies have been studied.

Those strategies involved the reduction of the CC rotational speed (hence, reduction of the SHe mass flow rate) with subcooled He bath at 4.2 K, or the adoption of alternative circuit layouts, such as one with the CCCs connected in series to the TF WP cooling channels, and another one featuring separate circuits for WPs and casings (both thermally coupled with the same He bath). The latter alternative layout, which requires additional CC and cryolines, resulted in approximately a 32% reduction of the CC power; moreover, also a reduction of the peak heat load to the thermal buffer is obtained by reducing the rotational speed of the casing circuit CC to ¼ of its nominal value during the pulsed heat load. For the alternative layout with TF WPs and TF casings hydraulically connected in series, and with a subcooled He bath at 4.2 K, a large 62% reduction of the CC power is obtained, with advantage of avoiding the additional CC and cryolines. However, a major drawback is that the

series connection between casings and conductors requires to slow down the rate of the cooldown transient. The most effective results, however, are obtained with a reduced (and constant) CC rotational speed and reduced total SHe flow rate such to have a $\Delta p \sim 1$ bar along the conductors cooling channels, with a subcooled He bath; in this case, in fact, the CC power consumption is 66% lower than that obtained for the reference configuration. However, this strategy requires an additional cold compressor to pump He vapor from the He bath, and the reduced CC pressure head causes a reduction of the temperature margin in the conductors. For the selection of the suitable configuration of the TF cooling circuit, also the economic feasibility of the different strategies must be assessed, which is however beyond the scope of the present work.

In perspective, a sizing analysis for the cold compressor needed in the case of a subcooled will be performed, and in case the buffer is not sufficient, some additional mitigation strategies for the smoothing of the power transferred to the refrigerator, involving suitable controls, will be investigated. Moreover, simulations for the other relevant transient, i.e. the TF cooldown in the cryoplant, will be performed. The development of system-level models for the cooling circuits of the poloidal field coils and central solenoid module coils is also foreseen.

CRediT authorship contribution statement

Fabrizio Lisanti: Formal analysis, Methodology, Software, Writing - Original Draft. **Morena Angelucci:** Project administration, Funding acquisition , Writing - Review & Editing. **Roberto Bonifetto:** Conceptualization, Methodology, Supervision, Writing - Review & Editing. **Frédéric Michel:** Project administration. **Davide Duri:** Project administration , Writing - Review & Editing. **Antonio Froio:** Conceptualization, Methodology, Supervision, Writing - Review & Editing. **Antonio Frattolillo:** Project administration, Funding acquisition. **Andrea Iaboni:** Formal analysis, Methodology. **Silvio Migliori:** Project administration, Funding acquisition. **Pascal Roussel:** Project administration. **Roberto Zanino:** Supervision.

Declaration of Competing Interest

The authors declare that they have no known competing financial interests or personal relationships that could have appeared to influence the work reported in this paper.

Data availability

The authors are unable or have chosen not to specify which data has been used.

References

[1] Ambrosino R. DTT-Divertor Tokamak Test facility: A testbed for DEMO. Fusion Eng Des 2021;167:112330.
[2] R. Martone, R. Albanese, F. Crisanti, P. Martin and A. Pizzuto, DTT Divertor Tokamak Test facility–Interim Design Report, ENEA, April 2019.
[3] Mazzitelli G, et al. Role of Italian DTT in the power exhaust implementation strategy. Fusion Eng Des 2019;146:932–6.
[4] G. Polli, "Divertor Tokamak Test facility Plant Integration Document (PID)," vol. v1.3, May 24, 2019.
[5] Roussel P, Hoa C, Lamaison V, Michel F, Reynaud P, Wanner M. DESIGN STATUS OF THE CRYOGENIC SYSTEM AND OPERATION MODES ANALYSYS OF THE JT-60SA TOKAMAK. AIP Conf Proc April 2010;1218(1):1445–7.
[6] Bonifetto R, Casella F, Savoldi Richard L, Zanino R. Dynamic modeling of a supercritical helium closed loop with the 4C code. AIP Conf Proc 2012;1434(1):1743–50.
[7] Zanino R, Bonifetto R, Heller R, Savoldi Richard L. Validation of the 4C Thermal-Hydraulic Code against 25 kA Safety Discharge in the ITER Toroidal Field Model Coil (TFMC). IEEE Trans Appl Supercond 2011;21(3):1948–52.
[8] Zanino R, Bonifetto R, Hoa C, Savoldi Richard L. Verification of the predictive capabilities of the 4C code cryogenic circuit model. AIP Conf Proc 2014;1573(1):1586–93.
[9] Zanino R, Bonifetto R, Brighenti A, Isono T, Ozeki H, Savoldi L. Prediction, experimental results and analysis of the ITER TF insert coil quench propagation tests, using the 4C code. Supercond Sci Technol 2018;31(3):035004.
[10] Munson B, Rothmayer A, Okiishi T, Huebsch W. Fundamentals of Fluid Mechanics. 7th ed. John Wiley & Sons Inc; 2013.
[11] "Beyond Gravity website," [Online]. Available: https://www.beyondgravity.com/en/satellites/platform-mechatronics/satellite-multilayer-insulation. [Accessed June 2023].
[12] Bonifetto R, Di Zenobio A, Muzzi L, Turtu S, Zanino R, Zappatore A. Thermal-hydraulic analysis of the DTT Toroidal Field magnets in DC operation. IEEE Trans Appl Supercond June 2020;30(4).
[13] Mattsson SE, Elmqvist H, Otter M. Physical system modeling with Modelica. Control Eng Pract 1998;6(4):501–10.
[14] Casella F, Leva A. Modelica open library for power plant simulation: design and experimental validation. Proceeding of the 2003 Modelica conference. 2003.
[15] Casella F, Richter C. ExternalMedia: a library for easy re-use of external fluid property code in Modelica. Proceedings 6th International Modelica Conference. 2008.
[16] Villari R, Angelone M, Caiffi B, Colangeli A, Crisanti F, Flammini D, et al. Nuclear design of Divertor Tokamak Test (DTT) facility. Fusion Eng Des 2020;155:111551.
[17] Bessette D, Shatil N, Zapretilina E. Simulations of the ITER toroidal field coil operation with the VINCENTA code. IEEE Trans Appl Supercond 2006;16(2):795–8.
[18] B. Lagier, C. and Hoa e B. and Rousset, «Validation of an EcosimPro® model for the assessment of two heat load smoothing strategies in the HELIOS experiment,» *Cryogenics,* vol. 62, pp. 60-70, 2014.
[19] Zanino R, Bonifetto R, Hoa C, Savoldi Richard L. 4C modeling of pulsed-load smoothing in the HELIOS facility using a controlled bypass valve. Cryogenics 2013;57:31–44.